Scientific Research Publishing

Green and Sustainable Chemistry, 2026, 16(3), 69-92
https://www.scirp.org/journal/gsc
ISSN Online: 2160-696X
ISSN Print: 2160-6951

Structure of Single Crystals of (E)-1,3-diphenylprop-2-en-1-one (Chalcone) Synthesized with a Natural Phosphate-Based Catalyst

Jean-Baptiste Zoungrana[1], Hadi Hamadoum Goro[1], Brahima Sorgho[1*], Eric Ziki[2], Emmanuel Wenger[3], Boubié Guel[1], Lecomte Claude[3]

[1]Laboratory of Molecular Chemistry and Materials (LC2M), Joseph KI-ZERBO University, Ouagadougou, Burkina Faso
[2]Laboratory of Matter, Environmental and Solar Energy Sciences, Research Team: Crystallography and Molecular Physics, University Félix Houphouët-Boigny, Abidjan, Ivory Coast
[3]CRM2, CNRS-CNRS-University of Lorraine, Vandœuvre-lès-Nancy, France
Email: *sorghobrahima3@gmail.com

How to cite this paper: Zoungrana, J.-B., Goro, H.H., Sorgho, B., Ziki, E., Wenger, E., Guel, B. and Claude, L. (2026) Structure of Single Crystals of (E)-1,3-diphenylprop-2-en-1-one (Chalcone) Synthesized with a Natural Phosphate-Based Catalyst. *Green and Sustainable Chemistry*, **16**, 69-92.
https://doi.org/10.4236/gsc.2026.163005

Received: March 31, 2026
Accepted: June 9, 2026
Published: June 12, 2026

Abstract

Chalcones are phenolic compounds belonging to the flavonoid family, recognized for their multiple biological properties, including antioxidant, anti-inflammatory, antibacterial, antifungal, antiviral, and anticancer activities. This bioactive versatility has generated increasing interest in medicinal chemistry, where they are explored as promising sources of new therapeutic agents. The present study focused on the synthesis of an (E)-chalcone via Claisen-Schmidt condensation, catalysed by natural phosphates from Burkina Faso, followed by an in-depth structural characterization using spectroscopic analyses (FT-IR, ^{1}H NMR) and crystallographic analysis by single-crystal X-ray diffraction. The FT-IR spectra highlight the characteristic bands of the main functional groups, particularly C=O, C=C, and Csp^2-H, confirming the presence of a well-established conjugated system. The trans (E) configuration of the *α,β*-unsaturated double bond is validated by the high coupling constant observed in ^{1}H NMR. Furthermore, crystallographic analysis reveals that the compound crystallizes in the orthorhombic system within the $Pca2_1$ space group, with a spatial organization mainly governed by the planarity of the aromatic rings. This structural feature may be advantageous for the design and development of new potent therapeutic agents, building on previously established strategies.

Keywords

Synthesized Chalcone, X-Ray Diffraction, Crystal Structure, Single Crystal

1. Introduction

Chalcones constitute a class of α,β-unsaturated carbonyl compounds of natural or synthetic origin, exhibiting a wide range of pharmacological and industrial applications. These molecules play a key role as privileged intermediates in the biosynthesis of flavonoids and in the synthesis of various biologically active heterocyclic compounds [1] [2]. Their therapeutic use is rooted in a millennia-old tradition based on the use of plant resources for the treatment of various diseases. Contemporary studies have demonstrated multiple pharmacological properties, including anticancer [3]-[5], antifungal [6], anti-inflammatory [7], antidiabetic, chemopreventive, antioxidant [8], and antimicrobial activities [9]. These features have generated increasing interest within the scientific community, driving intensive research into organic synthesis strategies and structural modifications of these compounds [10]. Chemists regard these compounds as a promising field of investigation, conducive to the development of new therapeutic entities and innovative functional materials [11].

Moreover, in a societal context marked by growing awareness of environmental pollution issues, the adoption of green synthetic methods has become a major priority in chemical research [12]. Traditionally, chalcones are synthesized via condensation reactions catalysed in basic or acidic media. Although these compounds, belonging to the class of α,β-unsaturated ketones, are readily accessible through classical routes, an increasing number of new synthetic approaches have recently been developed [1] [13]. These methodological advances stem both from the sustained interest in their versatile biological properties and from the recent development of innovative catalysts associated with optimized reaction conditions, combining enhanced efficiency with environmental compatibility. In this context, heterogeneous catalysts have emerged as preferred tools in both industrial processes and fundamental research. Their ability to selectively activate chemical reactions while remaining insoluble in the reaction medium offers major operational advantages, particularly in terms of recovery, reuse, and waste reduction. Among these catalysts, those derived from natural phosphates stand out for their potential to promote more sustainable processes [14]. Reactions catalysed by these phosphates have been investigated from various perspectives, highlighting their versatility and efficiency [15]-[18]. These transformations include, in particular, the hydration of nitriles to amides, a key step in amine chemistry [19]. Transesterification, essential for biodiesel production, has also been widely studied. Furthermore, the synthesis of chalcones, important intermediates in the production of bioactive compounds, illustrates the relevance of natural phosphates as catalysts.

In this context, numerous studies have focused on the Claisen-Schmidt condensation, with chalcone synthesis being the most commonly investigated reaction due to its importance in organic chemistry and pharmacology. Since 2010, the scientific literature on Claisen-Schmidt condensations has grown significantly, reaching a peak in 2012 with an average of more than 200 publications per year until

2018 [20]. This trend reflects increasing interest in carbon-carbon bond formation, leading to compounds of biological and pharmacological importance, which are crucial for the development of new therapeutic agents. Furthermore, the adoption of heterogeneous catalysis has reinforced the relevance of these reactions within the framework of green chemistry. Despite the large number of studies devoted to chalcones, an in-depth analysis of their structure after synthesis catalysed by natural phosphates remains insufficiently explored. This gap in the scientific literature highlights the need for further fundamental research in this area. Numerous works have been devoted to the characterization and understanding of the properties of these compounds, as well as to the optimization of synthesis processes. Crystallization and determination of crystal structure are essential steps in such investigations.

The present study highlights the synthesis of chalcones via Claisen-Schmidt condensation, a well-established chemical process known for its ability to generate complex aromatic compounds. The objective of this study is, on the one hand, the controlled synthesis of chalcones in the presence of a heterogeneous catalyst based on natural phosphate, and, on the other hand, their in-depth physicochemical characterization. This dual approach aims to establish a precise correlation between the molecular structure of the compounds and their properties, using a set of advanced analytical techniques. In this perspective, the adopted synthetic strategy involves catalysts based on natural phosphates from Burkina Faso. These materials, recognized for their abundance, eco-friendly nature, and catalytic efficiency, fit within an approach focused on the valorisation of local resources and sustainable chemistry. We will explore the optimal experimental conditions as well as the advantages of using these natural catalysts, which not only facilitate the reaction but also contribute to more environmentally friendly synthetic methods.

By analysing the obtained results, this study aims to establish a relationship between the unique properties of the synthesized chalcones and the characteristics of the natural phosphates used, thereby opening the way for potential applications in the pharmaceutical and agrochemical fields. Structural analysis, carried out by single-crystal X-ray diffraction, is particularly emphasized, as this technique provides precise information on the atomic arrangement and molecular configuration of the synthesized chalcones [21]-[23]. This approach not only deepens the understanding of the properties of these compounds but also opens new perspectives for their development and application in various fields, such as medicinal chemistry and agrochemistry. Indeed, the synthesis of chalcones catalysed by natural phosphates could lead to the discovery of new therapeutic agents, given the promising biological properties of these molecules. Furthermore, this method proves to be an effective complement to analyses performed by infrared spectroscopy and nuclear magnetic resonance (NMR) on the synthesized chalcones. By integrating X-ray diffraction techniques, a more comprehensive view of the molecular structure can be obtained, allowing correlations between structural features and observed biological activities. This synergy between different analytical methods

strengthens our understanding of chalcones and promotes their use in innovative applications.

2. Experimental

2.1. Origin of the Sample

The sample used in this study originates from the Kotchari phosphate deposit, located 70 km northeast of Arly and 40 km south of Diapaga, in eastern Burkina Faso. Kotchari lies between 11˚30' and 11˚55' north latitude and between 1˚25' and 2˚00' east longitude, within the rural commune of Tansarga, in the southern part of Tapoa Province (Figure 1). The phosphate rocks are mainly composed of carbonate-fluorapatite (francolite), $(Ca_5(PO_4)_{2.5}(CO_3)_{0.5}F)$; hydroxylapatite, a pentacalcium tris(phosphate) hydroxide, $(Ca_5(PO_4, CO_3)_3(OH))$; as well as alpha-quartz (α-SiO_2) [24].

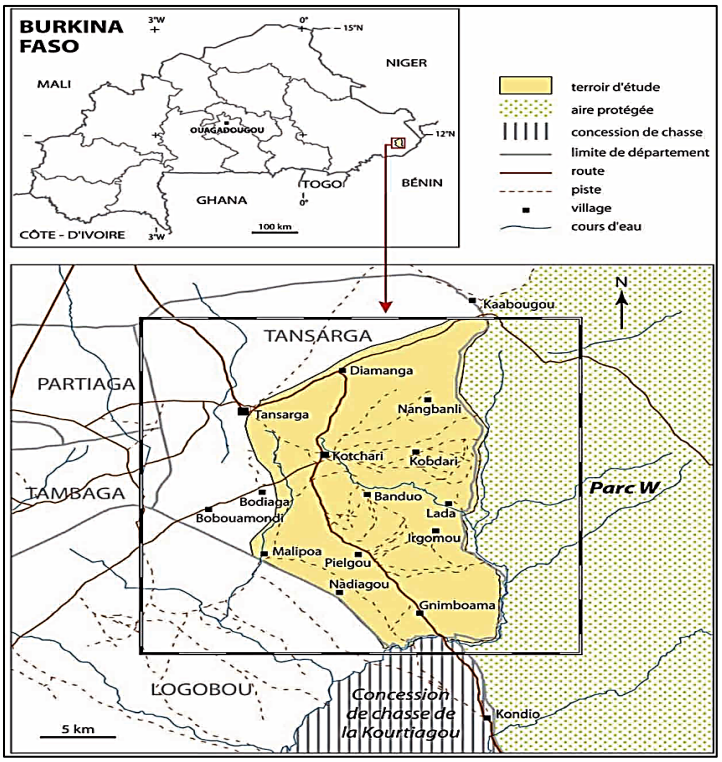

Figure 1. Location of the sample collection site.

2.2. Thermal Activation of Natural Phosphates

The collected natural phosphate was subjected to mechanical pretreatments structured in several stages. First, a preliminary crushing step was carried out to reduce the initial particle size of the material from the centimeter scale to the millimeter scale. This size reduction was performed using a jaw crusher to ensure fragment homogeneity. The resulting material was then ground using a ROC IMPACT ball mill to reach a micrometric particle size, thereby increasing the specific surface area of the particles, which is essential for catalytic applications.

The particle size distribution was determined by differential sieving using a column of standardized sieves (AFNOR X11-501). The selected fraction, ranging from 63 to 125 µm, complies with international standards for heterogeneous catalysts (ISO 3310-1) and was isolated for further studies. This size range optimizes surface properties while minimizing mass transfer effects during catalyzed reactions.

Subsequently, the phosphatic material was subjected to calcination at 900˚C for two hours, followed by a washing step aimed at removing a large portion of organic matter as well as residual carbonates. A water leaching step was then performed to extract lime and magnesia formed during calcination. The treated sample was dried in an oven for six hours to eliminate any residual moisture.

A portion of the pretreated natural phosphate was then subjected to a second calcination at 900˚C for two hours in a furnace to activate the material, hereafter referred to as the catalyst. This treatment ensures the dehydration and decarbonation of the precursors and promotes the formation of stable crystalline phases. After cooling, the material was ground and sieved (<80 µm), yielding a catalyst with optimal structural and textural properties for catalytic applications.

2.3. Synthesis of Chalcone

The synthesis of chalcone was carried out by reacting acetophenone (2 mL, 1.7×10^{-2} mol) with benzaldehyde (1.8 mL, 1.7×10^{-2} mol) in 5 mL of distilled water. The experiments were performed at room temperature in the presence of 1 g of catalyst (Scheme 1).

At the end of the reaction, the mixture was heated to approximately 60˚C to ensure complete dissolution of the product. The heterogeneous catalyst was removed by filtration. The filtrate containing the chalcone was then cooled in an ice bath under stirring for one hour, promoting precipitation. The precipitate was collected by vacuum filtration, washed with ice-cold water and then with cold ethanol (5 mL) to remove impurities, and air-dried.

Finally, the crude product was purified by recrystallization in 5 mL of ethanol.

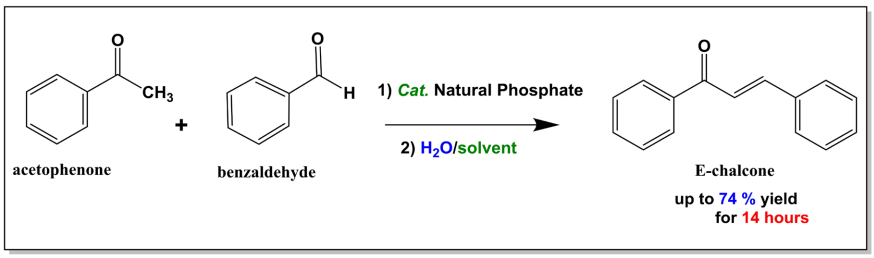

Scheme 1. General method for the synthesis of chalcone.

2.4. Characterization Methods

Scanning electron microscopy (*SEM*)

The morphology of the different powdered samples was examined using a Microspec-WDX 600/OXFORD microscope. The operating voltage was set at 20 kV,

allowing magnifications of up to 30,000×. The samples, previously ground to a particle size below 100 µm, were mounted on double-sided adhesive tape fixed onto the sample holder. The assembly was then coated with a thin layer of gold (Au/Ag) to render it conductive before observation.

Specific surface area measurement

To measure the specific surface area, the sample was pretreated. This pretreatment consisted of degassing and dehydrating the phosphate at 250˚C for 24 hours to remove all previously adsorbed gases. Nitrogen was used as the probe gas in this study. An N_2 adsorption-desorption isotherm was obtained. The measurements were carried out at 77 K, corresponding to the boiling temperature of nitrogen.

The specific surface area and total pore volume of the different materials were estimated from the N_2 adsorption-desorption isotherms at the boiling temperature of liquid nitrogen (77 K). The surface area of the phosphate was determined using a Bel Sorp-max instrument controlled by Bel Japan Inc. software.

X-ray photoelectron spectroscopy (XPS)

The XPS spectra of our samples were recorded using an ESCALAB 250 spectrometer (Thermo Electron), equipped with a monochromatic Al Kα radiation source (1486.6 eV), operating at a power of 150 W (15 kV, 10 mA). Measurements were carried out directly on powdered samples deposited on a sample holder, with an analysis area of approximately 500 µm in diameter, in an ultra-high vacuum chamber (pressure ≤ 2×10^{-9} Torr). The analysis depth ranges between 3 and 10 nm.

Infrared spectroscopy (IR)

Fourier transform infrared (FT-IR) spectroscopy analysis was carried out using a Thermo Fisher Scientific spectrometer, equipped with attenuated total reflectance (ATR), in the frequency range of 400 - 4000 cm^{-1}.

Proton nuclear magnetic resonance (^1H NMR)

Nuclear magnetic resonance (NMR) experiments were carried out using a Bruker Avance 600 MHz spectrometer for ^1H NMR. Chemical shift values were expressed in parts per million (ppm) on the delta (δ) scale, while coupling constants (J) were measured in hertz (Hz).

X-ray diffraction (XRD)

Single-crystal X-ray diffraction is a technique that provides precise information on atomic arrangement, based on the interaction of X-rays with the crystal lattice. A suitable single crystal was carefully selected and analysed using a Bruker D8 VENTURE diffractometer (Mo-Kα, λ = 0.71073 Å) equipped with a PHOTON II CPAD detector, with an angular scan range in θ from 2.4˚ to 30.5˚.

A total of 30,161 reflections were measured, of which 3276 were identified as independent, with a reproducibility factor R(int) of 0.070. Refinement was carried out on F^2 using the SHELXL-2018/3 program, applying an empirical weighting scheme [25]. Non-hydrogen atomic parameters were refined freely with anisotropic displacement parameters, while hydrogen atoms were positioned using a geometric model and refined under constraints.

The R_1 factor was 4.3% for significant reflections ($I > 2\sigma(I)$), and the weighted factor wR_2 was 10.8%, with a maximum residual electron density of 0.26 eÅ^{-3}. The absolute structure was determined from 949 Bijvoet reflection pairs, with a Flack parameter x = 0.1 (8), confirming the assigned configuration [26].

Details of the crystal data and refinement are presented in **Table 1**.

Table 1. Crystalline data and structure refinement.

Empirical formula	$C_{15}H_{12}O$
Formula weight	208.25
Temperature	100 (2) K
Wavelength	0.71073 Å
Crystal system	Orthorhombic
Space group	*Pca2₁*
Cell dimensions	a = 11.4211 (4) Å b = 12.7451 (4) Å c = 7.4518 (3) Å
Volume	1084.71 (7) Å^3
Z	4
Density (calculated)	1.275 mg·m^{-3}
Absorption coefficient	0.08 mm^{-1}
F(000)	440
Crystal size	0.4 × 0.27 × 0.25 mm^3
Theta range for data collection	2.4˚ - 30.5˚
Index ranges	−16 ≤ h ≤ 16 −18 ≤ k ≤ 18 −10 ≤ l ≤ 10
Reflections collected	30,161
Independent reflections	3276 Rint = 0.070
Refinement method	Full-matrix least-squares on F^2
Data/restraint/parameters	3276/1/146
Goodness-of-fit on F^2	1.02
Final R indices	R_1 = 0.043, wR_2 = 0.108
Largest diff. peak and hole	−0.27e Å^{-3}

3. Results and Discussion

3.1. Catalyst Characterization

The image of raw natural phosphate (**Figure 2**) shows a heterogeneous structure, consisting of an assembly of irregular agglomerates and fine particles, characteristic of a material rich in mineral impurities and organic matter [27].

In contrast, after calcination, the calcined phosphate exhibits a more homogeneous morphology with more well-defined grains. This results from the decomposition of carbonates, the removal of impurities during thermal treatment, and the stabilization of crystalline phases [28].

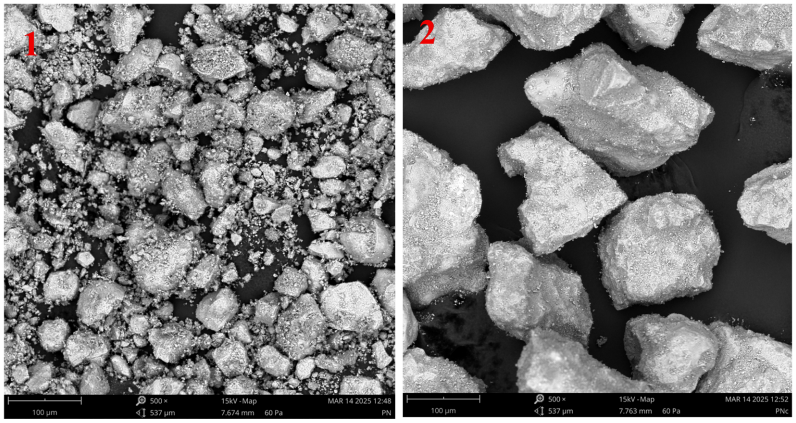

Figure 2. SEM image (500×) before (1) and after (2) catalyst preparation.

Table 2 shows a significant decrease in calcium (Ca) content after calcination (48.2% → 39.66%). Calcination may reduce the surface concentration of certain calcium-containing impurities following post-calcination washing [29]. As the main element of the phosphate phase, variations in calcium content directly reflect structural modifications and material density, particularly those induced by calcination, which can affect the compactness of the crystal lattice and the exposure of active surfaces.

The phosphorus (P) content decreases slightly after calcination (22.21% → 19.23%), indicating good stability of phosphorus during the treatments [29] [30]. The silicon (Si) content increases significantly after calcination (21.68% → 25.57%), which may result from better exposure of silicate phases at the surface or from element redistribution induced by thermal treatment.

Moreover, iron (Fe) and aluminum (Al) contents also increase after calcination, rising from 2.74% to 4.99% and from 5.04% to 7.77%, respectively. These changes may be explained by a relative concentration effect following the mass loss of other elements or by improved detection due to structural reorganization.

Table 2. Surface composition of raw phosphate and catalyst in atomic percent (at.%).

Elements	Raw phosphate (at.%)	Catalyst (at.%)
Ca	48.20	39.66
P	22.21	19.23
Si	21.68	25.57
Fe	2.74	4.99
Al	5.04	7.77
K	0.13	0.84

The specific surface area and pore volume of the raw phosphate (**Table 3**) are 167.33 m^2/g and 0.14 cm^3/g, respectively, indicating a porous texture favourable for catalytic activity [31]. However, after calcination at 900˚C (catalyst), a noticeable decrease in these values was observed, with the specific surface area reduced to 140.99 m^2/g and the pore volume to 0.12 cm^3/g.

The decrease in specific surface area can be interpreted as a consequence of progressive particle fusion. Under the effect of heat, the mobility of solid species increases, promoting particle agglomeration and grain sintering, which leads to crystal growth. This compaction process results in a reduction in the number of accessible pores and, consequently, a significant loss of specific surface area [32].

From a thermodynamic perspective, calcination provides the energy required to overcome kinetic barriers that maintain amorphous or mesoporous structures. The system then tends to minimize its free energy by favouring crystal growth and structural reorganization, leading to matrix densification and the gradual disappearance of micropores. This phenomenon may cause pore closure or reorganization, thereby limiting the accessibility of adsorption sites.

Moreover, certain amorphous phases, characterized by a high specific surface area, may transform into denser crystalline phases, further contributing to the decrease in surface area. This drastic reduction is generally attributed to the progressive disappearance of micropores, structural reorganization, and crystal growth induced by temperature, all of which lead to matrix densification.

This transformation, well documented by H. H. Lim *et al.* (2001), A. K. Özer *et al.* (2006), and T. F. Al-Fariss *et al.*, highlights the decisive influence of calcination conditions on the evolution of porous texture and, consequently, on the adsorption properties and potential catalytic activity of these materials [33]-[35].

It is important to note that although this reduction may appear unfavourable, it can also lead to improved thermomechanical stability of the catalyst. Indeed, larger grain size enhances resistance to erosion and degradation under reaction conditions. However, it remains essential to strike a balance to preserve optimal catalytic activity.

Table 3. Measurement of specific surface area, pore volume, and pore diameter.

Samples	Specific surface area B.E.T. (m^2/g)	Pore volume (cm^3/g)	Pore diameter (nm)
Phosphate brut	167.33	0.14	2.10
Catalyseur	140.99	0.12	2.13

The detailed analysis of the XPS spectrum of the catalyst (**Figure 3**) reveals the presence of several characteristic chemical species likely to play a key role in the physicochemical properties of the material. The predominant peak located at 532 eV (O 1s) indicates a high concentration of oxygen-containing groups, mainly associated with hydroxyl (-OH) and carbonyl (C=O) functionalities.

This high oxygen content is of great importance, as it governs surface chemical interactions and can significantly influence the reactivity of the material in

heterogeneous catalysis. Oxygen plays a crucial role in the adsorption and desorption processes of reactants, directly affecting the efficiency and kinetics of catalytic reactions. An oxygen-enriched surface promotes the formation of active bonds with reactive species, which can not only accelerate chemical transformations but also improve product selectivity [36] [37]. This behavior is particularly important in catalytic systems where surface reactivity is a key factor in optimizing overall catalyst performance.

Furthermore, the presence of a fluorine signal (F 1s, ~685 eV) suggests structural incorporation of fluorine into the matrix, supporting the hypothesis of carbonate-fluorapatite ($Ca_5(PO_4)_{2.5}(CO_3)_{0.5}F$) formation. The detection of iron (Fe 2p, 710 eV), although weak, indicates the presence of metallic traces, likely in the form of iron oxide (Fe_2O_3). Aluminum (Al 2p, 75 eV) is most likely present as alumina (Al_2O_3). Even at low concentrations, these impurities may influence the material's properties, particularly in terms of chemical reactivity and thermal stability.

The presence of phosphorus (P 2s, 190 eV) indicates the incorporation of phosphate groups (PO_4^{3-}) and/or P-O bonds, which are key elements in modulating surface properties and chemical interactions of the material [38]. These phosphate groups also open promising prospects in heterogeneous catalysis and biomedical applications due to their ability to interact with metal ions or biomolecules. Indeed, phosphate groups exhibit a strong interaction capacity with metal ions and biomolecules, which can enhance catalytic efficiency and support the development of biocompatible materials. This versatility highlights their key role in the design of functional materials adapted to complex environments [39].

The Si 2p peak at 155 eV suggests the presence of silicon in a specific chemical state, potentially associated with phosphate groups or other structures within the catalyst matrix. The identification of these chemical species within the catalyst underscores its potential for advanced applications, particularly in heterogeneous catalysis and multifunctional systems.

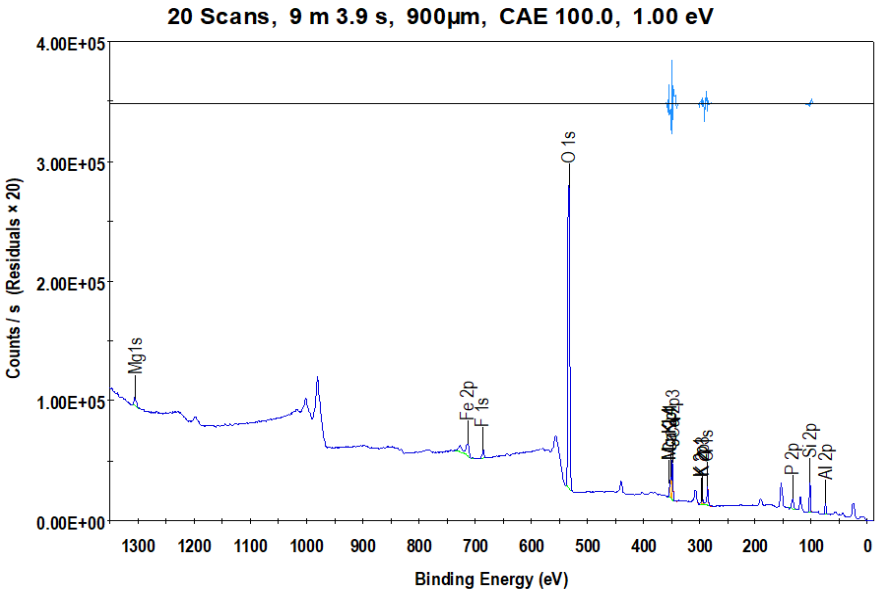

Elemental ID and Quantification

Name	*Peak BE*	*Atomic %*
O 1s	532.2	58.46
Si 2p	103.0	12.76
C 1s	285.1	10.32
Al 2p	74.7	7.01
Ca 2p³	347.7	4.03
P 2p	133.7	3.09
Fe 2p	712.4	1.52
F 1s	685.3	1.25
Mg 1s	1305.1	0.99
K 2p³	293.6	0.56

Figure 3. XPS spectrum of the catalyst.

3.2. Characterization of the Synthesized Product

The synthesized product obtained after recrystallization appears as yellow crystals (**Figure 4**). This morphological characteristic generally indicates a homogeneous chemical composition and a high degree of purity. Furthermore, the melting point of 54˚C, which is in line with the expected values for this type of compound, confirms the quality of the product obtained and the effectiveness of the purification process used.

A single-crystal X-ray diffraction study was carried out to analyze the structure of this compound.

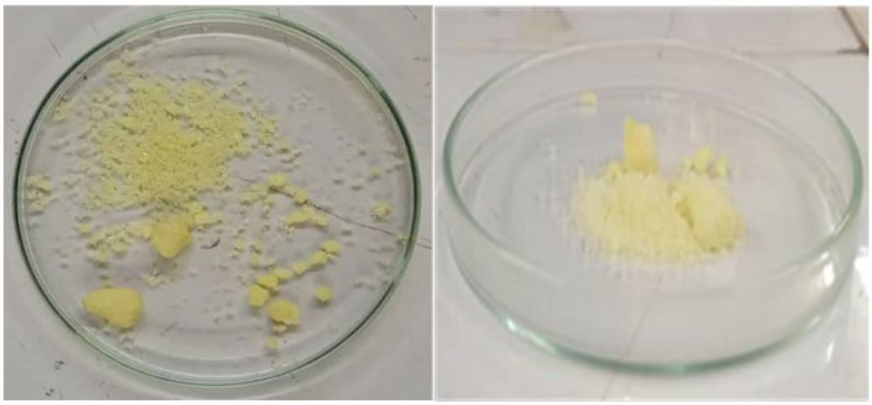

Figure 4. Synthesized product

3.3. FT-IR Spectrum

Figure 5 shows the FT-IR spectrum of the synthesized product, highlighting a characteristic band at 1662 cm^{-1} corresponding to the stretching vibration of the carbonyl group (C=O) [40] [41]. The band observed at 1604 cm^{-1} confirms the presence of an olefinic carbon-carbon double bond (C=C), while the band at 1500 cm^{-1}

is attributed to an aromatic C=C bond [40].

In addition, the spectrum reveals two weak absorption bands at 3240 and 3195 cm^{-1}, associated with Csp^2-H bonds [42]. The FT-IR analysis confirms that the obtained product is a chalcone, based on the characteristic bands related to its functional groups (C=O, C=C, and Csp^2-H).

The low multiplicity and moderate intensity of the bands corresponding to the stretching vibrations of aliphatic C-H bonds, observed at frequencies above 3000 cm^{-1}, may be attributed to a decrease in electron density on the carbon atoms [43] [44]. This decrease is accompanied by a reduction in the dipole moment associated with these bonds, resulting in weaker infrared absorption.

The carbonyl group (C=O) is distinguished by its strong spectroscopic sensitivity, due to charge transfer between electron donors and acceptors within this group [45]. This results in an intense absorption band in the infrared spectrum. This behaviour is also related to its high dipole moment, characteristic of a highly polar bond, reinforced by multiple bonding and possible π-π interactions between carbon and oxygen orbitals.

Furthermore, the band observed in the region between 1620 and 1500 cm^{-1}, attributed to the C=C group, is consistent with theoretical values [44]. It indicates effective conjugation between the C=C double bond and the carbonyl group (C=O), promoting electron delocalization within the conjugated system [46] [47].

The presence of conjugated π-systems in the structure of chalcones plays a fundamental role in their activity, facilitating electron delocalization required for the absorption of reactive oxygen species and interaction with bacterial targets.

In contrast, the peaks below 1000 cm^{-1} correspond to out-of-plane bending vibrations, also known as wagging vibrations [13]. These vibrations occur when bond angles change without significant variation in interatomic distances.

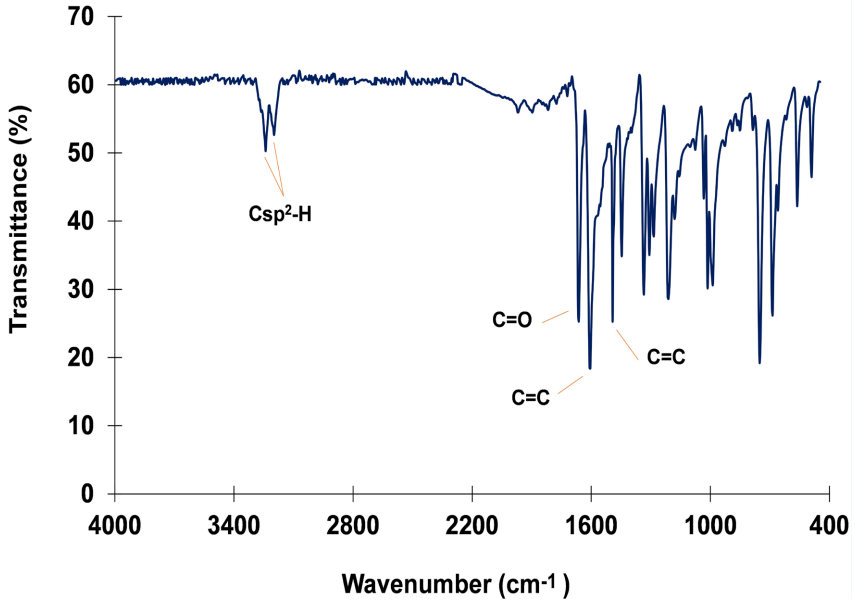

Figure 5. FT-IR spectrum of the synthesized product.

3.4. ^{1}H NMR Spectra

The ^{1}H NMR spectrum (500 MHz, DMSO-d_6) of the synthesized product (Figure 6) shows seven signals corresponding to seven distinct protons. This spectrum reveals the presence of aromatic protons, with characteristic multiplets and doublets in the range of 7.48 to 8.17 ppm.

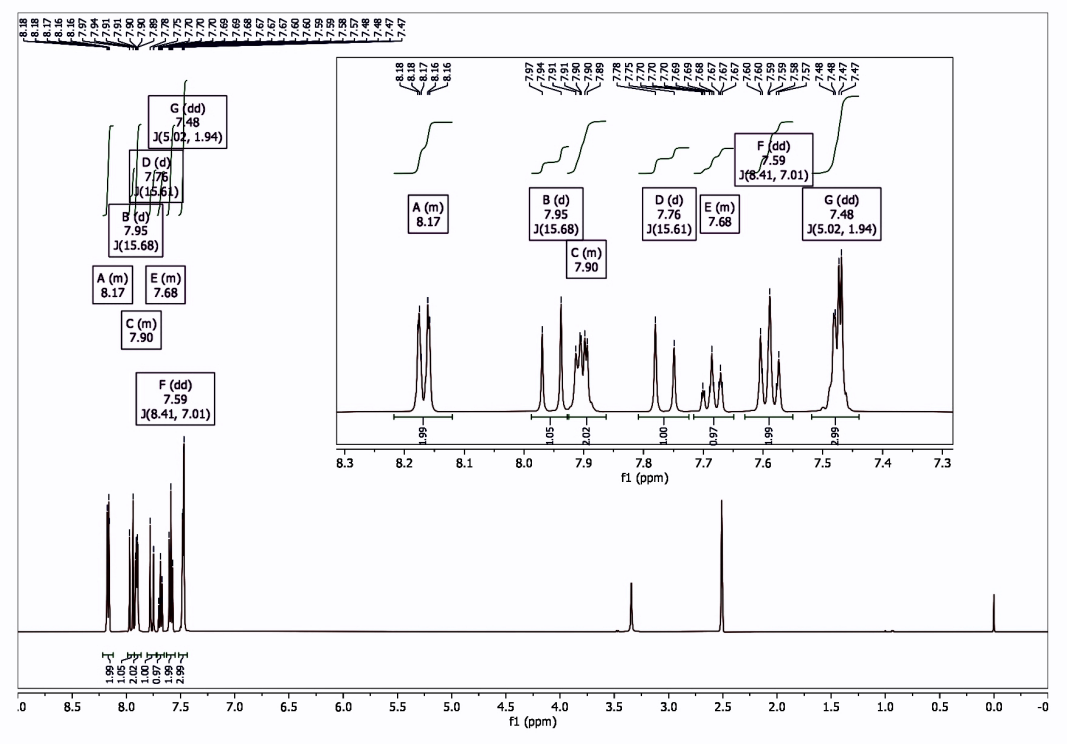

Figure 6. ^{1}H NMR spectrum (600 MHz) of the synthesized product.

A multiplet at 7.48 ppm corresponds to three aromatic protons (H3, H4, H5), indicating meta and para couplings. A doublet of doublets at 7.59 ppm (J = 8.41 and 7.01 Hz) is assigned to protons H3' and H5', typical of meta positions on an aromatic ring. An isolated multiplet at 7.68 ppm corresponds to proton H4', located at the para position.

Two well-resolved vinylic doublets are observed: one at 7.76 ppm (J = 15.61 Hz), attributed to Hα, and the other at 7.95 ppm (J = 15.68 Hz), attributed to Hβ. In addition, multiplets at 7.90 ppm (2H) correspond to protons H2 and H6, while those at 8.17 ppm (2H) are assigned to protons H2' and H6', located at meta and ortho positions, respectively (Figure 7).

The ^{1}H NMR spectrum of chalcone clearly shows two characteristic doublets corresponding to the vinylic protons Hα and Hβ. The large coupling constant (~15 Hz) suggests a trans configuration of the C=C double bond between Hα and Hβ, thus confirming the presence of a symmetric aromatic system as well as a trans α,β-unsaturated double bond [48].

This trans configuration is particularly favourable for the synthesis of (E)-

chalcone derivatives, which are recognized for their significant potential as anti-cancer, antibacterial, and antifungal agents [49]-[51]. In general, cis isomers are less stable than trans isomers [52], due to increased steric repulsion, conformational differences, higher potential energy, and distinct physical properties.

This difference in stability is of particular importance in organic chemistry, as it influences both the reactivity of compounds and their potential applications. These properties make such compounds promising candidates for further investigations in pharmaceutical research.

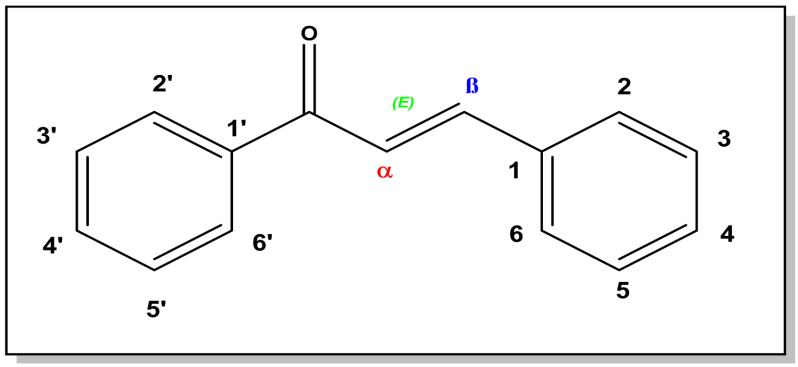

Figure 7. Structural representation of (E)-chalcone.

3.5. Crystal Structure

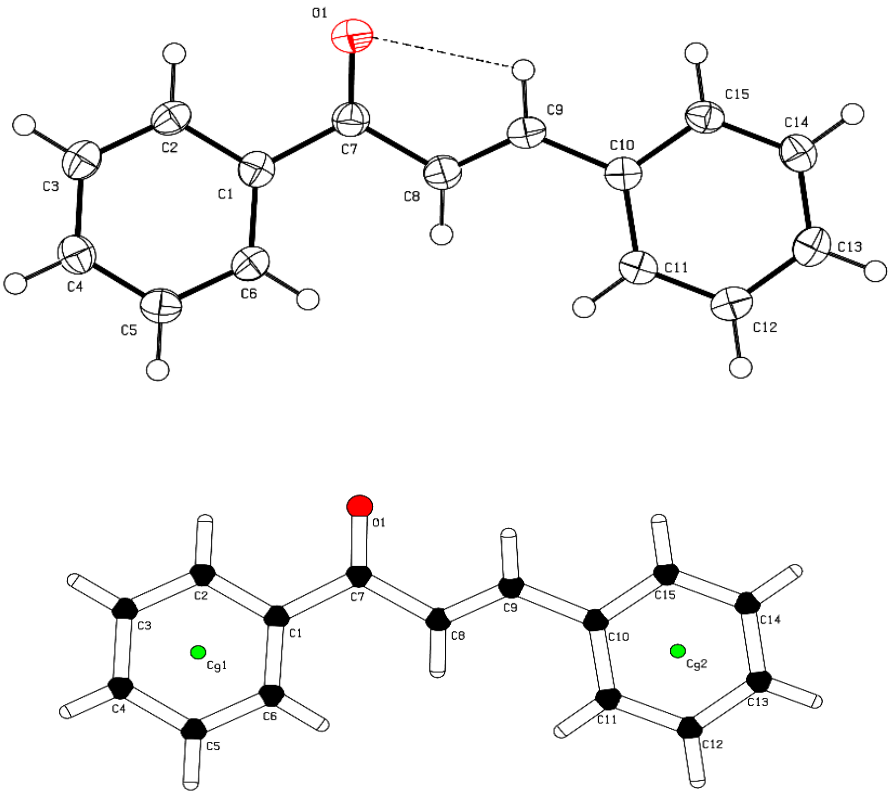

Figure 8. Molecular structure of a chalcone monomer.

The analysis of the molecular structure reveals the presence of various characteristic types of bonds, including aromatic rings, single and double bonds, as well as interactions involving hydrogen atoms (Figure 8).

The molecular structure is characterized by the presence of two nearly parallel benzene rings, where the intermolecular hydrogen bond of the type C9-H9···O1 is represented by a dashed line. Figure 9 illustrates the molecular arrangement in the (*a*, *b*) plane, while bond lengths and bond angles are given in Table 4 and Table 5, respectively.

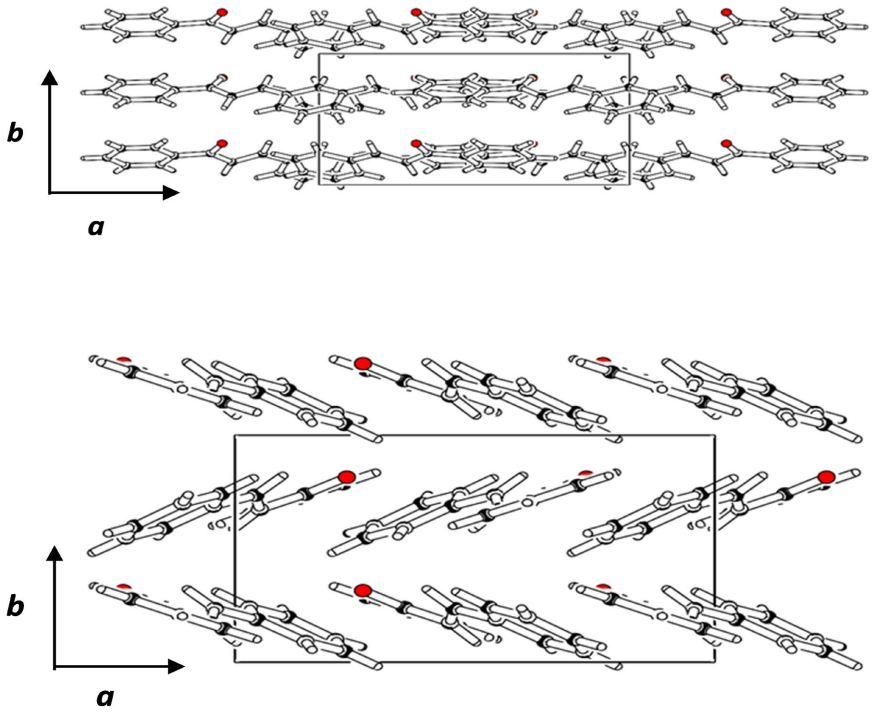

Figure 9. Molecular packing in the (*a*, *b*) plane.

Table 4. Bond lengths (Å).

Atoms	Bond length	Atoms	Bond length
C10-C11	1.398 (3)	C7-C8-H8	120.1
C10-C15	1.402 (3)	C5-C4-C3	119.79 (19)
C10-C9	1.462 (3)	C5-C4-H4	120.1
O1-C7	1.227 (2)	C3-C4-H4	120.1
C2-C3	1.385 (3)	C5-C6-C1	120.46 (19)
C2-C1	1.397 (3)	C5-C6-H6	119.8
C2-H2	0.9500	C11-C10-C15	118.33 (18)
C1-C6	1.393 (3)	C11-C10-C9	122.87 (18)
C1-C7	1.498 (3)	C15-C10-C9	118.79 (17)
C9-C8	1.336 (3)	C3-C2-C1	120.42 (18)
C9-H9	0.9500	C3-C2-H2	119.8

Continued

C14-C15	1.388 (3)	C1-C2-H2	119.8
C14-C13	1.390 (3)	C13-C14-H14	119.9
C14-H14	0.9500	C9-C8-C7	119.79 (18)
C8-C7	1.484 (3)	C5-C4-C3	119.79 (19)
C11-C10-C15	118.33 (18)	C5-C4-H4	120.1
C11-C10-C9	122.87 (18)	C3-C4-H4	120.1
C15-C10-C9	118.79 (17)	C8-H8	0.9500
C3-C2-C1	120.42 (18)	C4-C5	1.385 (3)
C3-C2-H2	119.8	C4-C3	1.391 (3)
C1-C2-H2	119.8	C4-H4	0.9500
C6-C1-C2	119.02 (17)	C6-C5	1.387 (3)
C6-C1-C7	123.02 (17)	C6-H6	0.9500
C2-C1-C7	117.91 (17)	C12-C13	1.388 (3)
C8-C9-C10	127.43 (19)	C12-C11	1.389 (3)
C8-C9-H9	116.3	C12-H12	0.9500
C10-C9-H9	116.3	C15-H15	0.9500
C15-C14-C13	120.13 (18)	C3-H3	0.9500
C15-C14-H14	119.9	C5-H5	0.9500
C13-C14-H14	119.9	C13-H13	0.9500
C9-C8-C7	119.79 (18)	C11-H11	0.9500
C9-C8-H8	120.1		

Table 5. Bond angles (˚).

Atoms	Bond angle	Atoms	Bond angle
C3-C2-C1-C6	−0.4 (3)	C9-C8-C7-C1	−158.82 (19)
C3-C2-C1-C7	−178.05 (19)	C6-C1-C7-O1	−174.6 (2)
C11-C10-C9-C8	−12.2 (3)	C2-C1-C7-O1	2.9 (3)
C15-C10-C9-C8	168.7 (2)	C6-C1-C7-C8	2.7 (3)
C10-C9-C8-C7	179.30 (19)	C2-C1-C7-C8	−179.80 (18)
C2-C1-C6-C5	−0.3 (3)	C3-C4-C5-C6	−1.0 (3)
C7-C1-C6-C5	177.19 (19)	C1-C6-C5-C4	1.0 (3)
C13-C14-C15-C10	−0.1 (3)	C11-C12-C13-C14	1.3 (3)
C11-C10-C15-C14	1.3 (3)	C15-C14-C13-C12	−1.2 (3)
C9-C10-C15-C14	−179.54 (18)	C13-C12-C11-C10	−0.1 (3)
C1-C2-C3-C4	0.5 (3)	C15-C10-C11-C12	−1.2 (3)
C5-C4-C3-C2	0.2 (3)	C9-C10-C11-C12	179.7 (2)
C9-C8-C7-O1	(3)		

The combined analysis of these results provides a comprehensive understanding of the molecular structure, which is essential for predicting its chemical behaviour and interactions in various contexts.

The synthesized compound crystallizes in the orthorhombic system, belonging to the space group $Pca2_1$. This crystalline configuration, determined from diffraction data, provides the basis for analyzing molecular interactions and the overall conformation of the compound in the solid state. The study of internal geometric parameters thus allows a better understanding of the factors contributing to the stability and organization of the crystal lattice [53].

The aromatic rings adopt a nearly parallel conformation, forming an angle of 11.70˚ between their mean planes, indicating a slight inclination within the crystal packing. This deviation from coplanarity suggests a certain structural flexibility, which may promote intermolecular interactions such as π-π stacking or C-H$\cdots\pi$ interactions.

The α,β-unsaturated keto group adopts a syn-periplanar (-sp) conformation, as evidenced by the torsion angle of 18.4 (3)˚ measured for atoms C9-C8-C7-O1. This nearly coplanar spatial arrangement facilitates electron delocalization between the double bond and the carbonyl group. Moreover, the olefinic double bond C9=C8, with a length of 1.336 (3) Å, exhibits an E configuration. This geometry is consistent with sp^2 hybridization of the involved carbon atoms, as confirmed by proton nuclear magnetic resonance (^{1}H NMR) spectroscopic data, which show a coupling constant characteristic of the -CH=CH- motif.

The C-H$\cdots\pi$ interactions observed in the crystal lattice confirm the involvement of aromatic rings in structural cohesion. Two significant contacts are identified: C12-H12···Cg2 (where Cg2 denotes the centroid of the benzene ring formed by atoms C10 to C15), with an H···Cg distance of 2.71 Å and a C-H···Cg angle of 133˚, and C15-H15···Cg2, characterized by an H···Cg distance of 2.70 Å and an angle of 144˚.

C-H$\cdots\pi$ interactions represent a class of non-covalent interactions that may be dominated either by electrostatic forces or dispersion interactions, depending on the acidity of the C-H group. They contribute to the stabilization of the crystal lattice by ensuring lateral anchoring between molecules through their aromatic rings [54]-[56].

The bond lengths measured within the two benzene rings-C1-C2 (1.397 Å), C2-C3 (1.385 Å), C3-C4 (1.391 Å), C4-C5 (1.385 Å), C5-C6 (1.387 Å), C6-C1 (1.393 Å), as well as C10-C11 (1.398 Å), C11-C12 (1.389 Å), C12-C13 (1.388 Å), C13-C14 (1.390 Å), C14-C15 (1.388 Å), and C15-C10 (1.402 Å)-all fall within a narrow range between 1.385 and 1.402 Å. These values are characteristic of aromatic C-C bonds, intermediate between single and double bonds, confirming π-electron delocalization throughout the ring [57] [58].

This near-equality of bond lengths attests to well-established aromaticity, conferring notable electronic stability to the molecule and playing a key role in the intermolecular interactions observed within the crystal lattice.

These remarkable properties of the synthesized product make it a particularly attractive scaffold for the design of therapeutic agents targeting specific biomolecules. Their ability to interact selectively with major biological targets makes them promising candidates for the development of new pharmacological entities [59]-[61]. Several chalcone derivatives have recently achieved pharmacological validation, illustrating their growing therapeutic potential. Among them, butein, sappanchalcone, and okanin stand out for their strong antioxidant activities [62]. Similarly, certain methylated chalcones have demonstrated notable efficacy in anticancer activity models [63]. Furthermore, dimethylamino-chalcones have shown significant activity as scavengers of the superoxide anion generated by stimulated human neutrophils, highlighting their potential role in controlling oxidative stress and inflammation [63].

The synthesised compound corresponds to the BZYACO structure previously reported in the literature [64]. This structural identity, confirmed by comparison of crystallographic data with those in the CSD database, fully validates our synthetic approach and highlights the remarkable efficacy of natural phosphate as an organic catalyst for the formation of this molecular entity.

The evaluation of the antibacterial and anticancer activities of this compound will be the subject of further studies.

4. Conclusions

All the experimental results obtained, combining spectroscopic analyses (FT-IR, ^{1}H NMR) and crystallographic data, allow a rigorous confirmation of the structure and nature of the synthesized compound, identified as an (E)-chalcone.

As part of this work on the synthesis of chalcones, no biological assays were conducted, as the primary objective focused on the preparation and structural characterisation of the compounds obtained. The evaluation of their potential antibacterial and anticancer activities will form the basis for future research, requiring specialised experimental protocols and technical resources beyond the scope of this study.

The evaluation of the antibacterial and anticancer activities of this compound will be the subject of further studies. The FT-IR spectrum highlights characteristic bands associated with the main functional groups, namely C=O, C=C, and Csp^2-H, indicating a well-established conjugated system. The presence of a strongly polar carbonyl group, as well as a conjugated double bond in a trans (E) configuration, is corroborated by the high coupling constant observed in ^{1}H NMR, confirming an α,β-unsaturated geometry.

Crystallographic analysis reveals that the compound crystallizes in the orthorhombic system, with a spatial organization governed by the planarity of the aromatic rings, the syn-periplanar conformation of the α,β-unsaturated keto moiety, and stabilizing C-H$\cdots\pi$ interactions. The near equality of C-C bond lengths confirms well-developed aromaticity, contributing to conformational stability.

This architecture, supported by π-electron delocalization, directly influences the

physicochemical properties and the bioactive potential of the compound. The trans configuration, more stable than the cis form, is particularly favourable for pharmacological applications, especially anticancer activity.

Thus, this comprehensive study not only provides full structural validation of the compound but also establishes fundamental insights for exploring its potential applications in medicinal chemistry, while highlighting the importance of combined approaches (spectroscopy and crystallography) in the characterization of bioactive molecules.

Owing to its intrinsic composition, potential thermal stability, and the possibility of structural modulation through targeted physicochemical treatments, the catalyst offers promising prospects for applications in sustainable processes, particularly in green chemistry. In this respect, this study provides a solid scientific foundation for the development of new catalytic materials derived from local resources and contributes to a rational and sustainable valorisation of national phosphate deposits.

Acknowledgements

The authors thank the Laboratory of Crystallography, Magnetic Resonance and Modeling (UMR CNRS 7036), affiliated with the University of Lorraine (Scientific Division "Molecular Chemistry and Physics") and the CNRS (Institute of Physics and Institute of Chemistry), for the crystallographic analyses performed by single-crystal X-ray diffraction.

Conflicts of Interest

The authors declare no conflicts of interest regarding the publication of this paper.

References

[1] Mulugeta, D. (2022) A Review of Synthesis Methods of Chalcones, Flavonoids, and Coumarins. *Science Journal of Chemistry*, **10**, 41-52.

[2] Sharma, S., Sandeep, K., Tania, B. and Jyoti, G. (2014) Review on Synthesis of Bioactive Pyrazoline Derivatives. *Chemical Science Transactions*, **3**, 861-875.

[3] Anto, R.J., Sukumaran, K., Kuttan, G., Rao, M.N.A., Subbaraju, V. and Kuttan, R. (1995) Anticancer and Antioxidant Activity of Synthetic Chalcones and Related Compounds. *Cancer Letters*, **97**, 33-37. https://doi.org/10.1016/0304-3835(95)03945-s

[4] Cong, H., Zhao, X., Castle, B.T., Pomeroy, E.J., Zhou, B., Lee, J., *et al.* (2018) An Indole-Chalcone Inhibits Multidrug-Resistant Cancer Cell Growth by Targeting Microtubules. *Molecular Pharmaceutics*, **15**, 3892-3900. https://doi.org/10.1021/acs.molpharmaceut.8b00359

[5] Ghosh, C., Gupta, N., Mallick, A., Santra, M.K. and Basu, S. (2018) Self-Assembled Glycosylated Chalcone-Boronic Acid Nanodrug Exhibits Anticancer Activity through Mitochondrial Impairment. *ACS Applied Bio Materials*, **1**, 347-355. https://doi.org/10.1021/acsabm.8b00089

[6] Lahtchev, K.L., Batovska, D.I., Parushev, S.P., Ubiyvovk, V.M. and Sibirny, A.A. (2008) Antifungal Activity of Chalcones: A Mechanistic Study Using Various Yeast Strains.

European Journal of Medicinal Chemistry, **43**, 2220-2228.
https://doi.org/10.1016/j.ejmech.2007.12.027

[7] Choi, D., Park, J.C., Lee, H.N., Moon, J., Ahn, H., Park, K., *et al.* (2018) *In Vitro* Osteogenic Differentiation and Antibacterial Potentials of Chalcone Derivatives. *Molecular Pharmaceutics*, **15**, 3197-3204.
https://doi.org/10.1021/acs.molpharmaceut.8b00288

[8] Mazzone, G., Galano, A., Alvarez-Idaboy, J.R. and Russo, N. (2016) Coumarin-Chalcone Hybrids as Peroxyl Radical Scavengers: Kinetics and Mechanisms. *Journal of Chemical Information and Modeling*, **56**, 662-670.
https://doi.org/10.1021/acs.jcim.6b00006

[9] Zhou, B. (2015) Diverse Molecular Targets for Chalcones with Varied Bioactivities. *Medicinal Chemistry*, **5**, 388-404. https://doi.org/10.4172/2161-0444.1000291

[10] Ivanova, Y., Momekov, G., Petrov, O., Karaivanova, M. and Kalcheva, V. (2007) Cytotoxic Mannich Bases of 6-(3-Aryl-2-Propenoyl)-2(3*H*)-Benzoxazolones. *European Journal of Medicinal Chemistry*, **42**, 1382-1387.
https://doi.org/10.1016/j.ejmech.2007.02.019

[11] Matsui, J., Nicholls, I.A., Karube, I. and Mosbach, K. (1996) Carbon-Carbon Bond Formation Using Substrate Selective Catalytic Polymers Prepared by Molecular Imprinting: An Artificial Class II Aldolase. *The Journal of Organic Chemistry*, **61**, 5414-5417.
https://doi.org/10.1021/jo9516805

[12] Dotta, D., Gastaldi, M., Fin, A., Barbero, N., Barolo, C., Cardano, F., *et al.* (2025) Chalcone Synthesis by Green Claisen-Schmidt Reaction in Cationic and Nonionic Micellar Media. *The Journal of Organic Chemistry*, **90**, 2915-2926.
https://doi.org/10.1021/acs.joc.4c02616

[13] Parol, V., Upadhyaya, V., Prabhu, A.N., Lokanath, N.K., Taher, M.A. and Naraharisetty, S.R.G. (2020) A Long-Chain Based Bromo and Methyl Substituted Chalcone Derivatives; Experimental and Theoretical Approach on Nonlinear Optical Single Crystals. *Materials Research Express*, **7**, Article 055101.
https://doi.org/10.1088/2053-1591/ab8b88

[14] Sheffer, H.E., Perry, R.L., Thimineur, R.J., Adams, B.T., Simonian, J.L., Zutty, N.L., *et al.* (1971) Aluminum Phosphate Catalyst. *Product R&D*, **10**, 362-365.
https://doi.org/10.1021/i360040a002

[15] Otomo, R., Yamaguchi, C., Iwaisako, D., Oyamada, S. and Kamiya, Y. (2019) Selective Dehydration of 1,2-Propanediol to Propanal over Boron Phosphate Catalyst in the Presence of Steam. *ACS Sustainable Chemistry & Engineering*, **7**, 3027-3033.
https://doi.org/10.1021/acssuschemeng.8b04594

[16] Zheng, B., Chen, H., Zhu, L., Hou, X., Wang, Y., Lan, Y., *et al.* (2019) Formal Asymmetric Cycloaddition of Activated *α,β*-Unsaturated Ketones with *α*-Diazomethylphosphonate Mediated by a Chiral Silver SPINOL Phosphate Catalyst. *Organic Letters*, **21**, 593-597. https://doi.org/10.1021/acs.orglett.8b03436

[17] Keane, T.P., Brodsky, C.N. and Nocera, D.G. (2019) Oxidative Degradation of Multi-Carbon Substrates by an Oxidic Cobalt Phosphate Catalyst. *Organometallics*, **38**, 1200-1203. https://doi.org/10.1021/acs.organomet.8b00337

[18] Song, D. (2017) Development of a Deactivation Model for the Dehydration of 2,3-Butanediol to 1,3-Butadiene and Methyl Ethyl Ketone over an Amorphous Calcium Phosphate Catalyst. *Industrial & Engineering Chemistry Research*, **56**, 11013-11020.
https://doi.org/10.1021/acs.iecr.7b02355

[19] Acharjee, A. and Saha, B. (2020) A Review of Some Catalysts and Promoters Used in

Organic Transformations. *Vietnam Journal of Chemistry*, **58**, 575-591. https://doi.org/10.1002/vjch.202000082

[20] Yadav, G.D. and Wagh, D.P. (2020) Claisen-Schmidt Condensation Using Green Catalytic Processes: A Critical Review. *Chemistry Select*, **5**, 9059-9085. https://doi.org/10.1002/slct.202001737

[21] Bitencourt, H.R., Pinheiro, J.C., Souza Filho, A.P.D.S., Moreira, S.G., Ayala, A.P. and Remédios, C.M.R. (2022) Monocristais de 1-(2'-hidroxifenil)-3-hidroxi-3-(4-metoxifenil)-propan-1-ona: Síntese, estrutura e propriedades vibracionais. *Research, Society and Development*, **11**, e10311931433. https://doi.org/10.33448/rsd-v11i9.31433

[22] López, Y., Belandria, L., Liew, S., Jamalis, J. and Delgado, G. (2019) Síntesis y caracterización estructural de un nuevo derivado pirazolínico. *Avances en Química*, **14**, 61-65. https://doi.org/10.53766/avanquim/2019.14.02.01

[23] Ravindrachary, V., Crasta, V., Bhajantri, R.F. and Poojari, B. (2005) Growth and Characterization of Chalcone Derivative Single Crystal. *Journal of Crystal Growth*, **275**, e313-e318. https://doi.org/10.1016/j.jcrysgro.2004.10.114

[24] Zoungrana, J., Sorgho, B., Bakouan, C., Sawadogo, S., Ouedraogo, R.D., Guel, B., *et al.* (2024) Mineralogical Study of Phosphate Rocks by Quantitative Rietveld Refinement. *Open Ceramics*, **18**, Article 100567. https://doi.org/10.1016/j.oceram.2024.100567

[25] Sheldrick, G.M. (2015) SHELXT-Integrated Space-Group and Crystal-Structure Determination. *Acta Crystallographica Section A*: *Foundations and Advances*, **71**, 3-8. https://doi.org/10.1107/s2053273314026370

[26] Parsons, S., Flack, H.D. and Wagner, T. (2013) Use of Intensity Quotients and Differences in Absolute Structure Refinement. *Acta Crystallographica Section B*: *Structural Science Crystal Engineering and Materials*, **69**, 249-259. https://doi.org/10.1107/s2052519213010014

[27] Boughzala, K. (2021) Study of the Physicochemical Properties of Natural Phosphate from the Oum Deposit, El Khecheb: Processing and Utilization of Byproducts from This Process. *Green and Applied Chemistry*, **11**, 179-202.

[28] Smahi, A., Solhy, A., Tahir, R., Sebti, S., Mayoral, J.A., García, J.I., *et al.* (2008) Preparation of α-Hydroxyphosphonates over Phosphate Catalysts. *Catalysis Communications*, **9**, 2503-2508. https://doi.org/10.1016/j.catcom.2008.07.005

[29] Attafi, I., Idres, A., Mekti, Z., Bouras, A., Benselhoub, A., Merzeg, F.A., *et al.* (2024) Analysis of Combined Processing Method of Phosphate Minerals from the Kef Essenoun Deposit. *Technology Audit and Production Reserves*, **2**, 12-19. https://doi.org/10.15587/2706-5448.2024.300739

[30] Ghamri, N.E., Kribaa, O.K., Zenkhri, L. and Djouama, H. (2023) Effect of Thermal Treatment on the Structural, Morphological, and Chemical Properties of Apatite Bioceramicsmaterials. *Digest Journal of Nanomaterials and Biostructures*, **18**, 531-545. https://doi.org/10.15251/djnb.2023.182.531

[31] Liu, B., Chen, Z., Liu, F. and Zhu, J. (2025) Characteristics of Modified Complex of Red Mud and Phosphogypsum and Its Soil Substrate Utilization. *Processes*, **13**, Article 972. https://doi.org/10.3390/pr13040972

[32] Benaddi, R. (2021) Synthesis and Characterization of Materials Derived from Natural Moroccan Phosphate and Their Applications in the Adsorption of Phenolic Compounds from Olive Pomace. Ph.D. Thesis, Sultan Moulay Slimane University.

[33] Özer, A.K., Gülaboglu, M.S., Bayrakçeken, S. and Weisweiler, W. (2006) Changes in Physical Structure and Chemical Composition of Phosphate Rock during Calcination in Fluidized and Fixed Beds. *Advanced Powder Technology*, **17**, 481-494.

https://doi.org/10.1163/156855206778440543

[34] Lim, H.H. and Gilkes, R.J. (2001) Beneficiation of Apatite Rock Phosphates by Calcination: Effects on Chemical Properties and Fertiliser Effectiveness. *Australian Journal of Soil Research*, **39**, 397-402. https://doi.org/10.1071/sr00005

[35] Al-Fariss, T.F., El-Aleem, F.A.A., Arafat, Y., El-Nagdy, K.A. and El-Midany, A.A. (2014) Low Solubility of Calcined Phosphate: Surface Area Reduction or Chemical Composition Change? *Particulate Science and Technology*, **32**, 80-85. https://doi.org/10.1080/02726351.2013.809395

[36] Slapničar, Š., Žerjav, G., Zavašnik, J., Roškarič, M., Finšgar, M. and Pintar, A. (2024) Novel TiO_2-Supported Gold Nanoflowers for Efficient Photocatalytic Nox Abatement. *Molecules*, **29**, Article 3333. https://doi.org/10.3390/molecules29143333

[37] Védrine, J. (2016) Heterogeneous Partial (amm)Oxidation and Oxidative Dehydrogenation Catalysis on Mixed Metal Oxides. *Catalysts*, **6**, Article 22. https://doi.org/10.3390/catal6020022

[38] Lin, R. and Ding, Y. (2013) A Review on the Synthesis and Applications of Mesostructured Transition Metal Phosphates. *Materials*, **6**, 217-243. https://doi.org/10.3390/ma6010217

[39] Zabirov, A.R., Serebrennikov, D.V., Kuvatova, R.Z., Filippova, N.A., Zilberg, R.A., Travkina, O.S., *et al.* (2025) Regulation of the Properties of the Hierarchical Porous Structure of Alumophosphate Molecular Sieves AEL by Reaction Gels Prepared with Different Templates. *Gels*, **11**, Article 297. https://doi.org/10.3390/gels11040297

[40] Patil, P.G., Melavanki, R., Radder, S.B., Kusanur, R., Hiremath, C.S., Patil, N.R., *et al.* (2021) Synthesis, Structural Characterizations, and Quantum Chemical Investigations on 1-(3-Methoxy-Phenyl)-3-Naphthalen-1-Yl-Propenone. *ACS Omega*, **6**, 25982-25995. https://doi.org/10.1021/acsomega.1c02688

[41] Radder, S.B., Melavanki, R., Hiremath, S.M., Kusanur, R., Khemalapure, S.S. and Jeyaseelan, S.C. (2021) Synthesis, Spectroscopic (FT-IR, Ft-Raman, NMR & UV-Vis), Reactive (ELF, LOL, Fukui), Drug Likeness and Molecular Docking Insights on Novel 4-[3-(3-Methoxy-Phenyl)-3-Oxo-Propenyl]-Benzonitrile by Experimental and Computational Methods. *Heliyon*, **7**, e08429. https://doi.org/10.1016/j.heliyon.2021.e08429

[42] Kassim Ali, S., Mohammad Murwih, A., Melati, K., *et al.* (2020) Design, Synthesis, Characterization, and Cytotoxicity Activity Evaluation of Mono-Chalcones and New Pyrazolines Derivatives. *Journal of Applied Pharmaceutical Science*, **10**, 20-36. https://doi.org/10.7324/japs.2020.10803

[43] Varrica, D., Tamburo, E., Vultaggio, M. and Di Carlo, I. (2019) ATR-FTIR Spectral Analysis and Soluble Components of PM10 and PM2.5 Particulate Matter over the Urban Area of Palermo (Italy) during Normal Days and Saharan Events. *International Journal of Environmental Research and Public Health*, **16**, Article 2507. https://doi.org/10.3390/ijerph16142507

[44] Michalak, I., Baśladyńska, S., Mokrzycki, J. and Rutkowski, P. (2019) Biochar from a Freshwater Macroalga as a Potential Biosorbent for Wastewater Treatment. *Water*, **11**, Article 1390. https://doi.org/10.3390/w11071390

[45] Zlotnikov, I.D., Krylov, S.S., Belogurova, N.G., Blinnikov, A.N., Kalugin, V.E. and Kudryashova, E.V. (2024) New Derivatives of Chalcones, Chromenes, and Stilbenoids, Complexed with Methyl-β-Cyclodextrin with Antioxidant Properties and Antibacterial Synergism with Antibiotics. *Biophysica*, **4**, 667-694. https://doi.org/10.3390/biophysica4040044

[46] Zhang, J. and Ma, H. (2019) Synthesis, Characterization, and Crystal Structures of

Imides Condensed with P-Phenylamino(Phenyl) Amine and Fluorescence Property. *Materials*, **12**, Article 1873. https://doi.org/10.3390/ma12111873

[47] Castro-Tamay, P., Villaman, D., Hamon, J. and Novoa, N. (2024) Isolated Dipolar ONN Schiff Base Regioisomers: Synthesis, Characterization and Crystallographic Study. *Molecules*, **29**, Article 5863. https://doi.org/10.3390/molecules29245863

[48] Gomes, M., Muratov, E., Pereira, M., Peixoto, J., Rosseto, L., Cravo, P., *et al.* (2017) Chalcone Derivatives: Promising Starting Points for Drug Design. *Molecules*, **22**, Article 1210. https://doi.org/10.3390/molecules22081210

[49] Al-Ghamdi, A.R., Ahmed, W.U., Al-Wabli, R.I., Al-Mutairi, M.S. and Rahman, A.F.M.M. (2025) Synthesis and Anticancer Evaluation of O-Alkylated (E)-Chalcone Derivatives: A Focus on Estrogen Receptor Inhibition. *International Journal of Molecular Sciences*, **26**, Article 833. https://doi.org/10.3390/ijms26020833

[50] Moreno, L.M., Quiroga, J., Abonia, R., Crespo, M.d.P., Aranaga, C., Martínez-Martínez, L., *et al.* (2024) Synthesis of Novel Triazine-Based Chalcones and 8,9-Dihydro-7h-Pyrimido[4,5-B][1,4]Diazepines as Potential Leads in the Search of Anticancer, Antibacterial and Antifungal Agents. *International Journal of Molecular Sciences*, **25**, Article 3623. https://doi.org/10.3390/ijms25073623

[51] Panchal, A.D. and Patel, P.M. (2012) Synthesis, Anti-Bacterial and Anti-Fungal Evaluation of Pyrazoline Derivatives. *Journal of Chemistry*, **9**, 1801-1809. https://doi.org/10.1155/2012/458035

[52] Albuquerque, H., Santos, C., Cavaleiro, J. and Silva, A. (2014) Chalcones as Versatile Synthons for the Synthesis of 5- and 6-Membered Nitrogen Heterocycles. *Current Organic Chemistry*, **18**, 2750-2775. https://doi.org/10.2174/1385272819666141013224253

[53] Kosar, N., Kanwal, S., Hamid, M.H.S.A., Ayub, K., Gilani, M.A., Imran, M., *et al.* (2023) Role of Delocalization, Asymmetric Distribution of *Π*-Electrons and Elongated Conjugation System for Enhancement of NLO Response of Open Form of Spiropyran-Based Thermochromes. *Molecules*, **28**, Article 6283. https://doi.org/10.3390/molecules28176283

[54] Kumar, M. and Balaji, P.V. (2014) C-H…pi Interactions in Proteins: Prevalence, Pattern of Occurrence, Residue Propensities, Location, and Contribution to Protein Stability. *Journal of Molecular Modeling*, **20**, Article No. 2136. https://doi.org/10.1007/s00894-014-2136-5

[55] Umezawa, Y., Tsuboyama, S., Honda, K., Uzawa, J. and Nishio, M. (1998) CH/π Interaction in the Crystal Structure of Organic Compounds. A Database Study. *Bulletin of the Chemical Society of Japan*, **71**, 1207-1213. https://doi.org/10.1246/bcsj.71.1207

[56] Stapf, M., Seichter, W. and Mazik, M. (2025) Crystal Structure and Hirshfeld Surface Analysis of Hexakis(acetoxymethyl)benzene. *Molbank*, **2025**, M2008. https://doi.org/10.3390/m2008

[57] Gu, H. and Lin, Q. (2025) Crystal Form Diversity of 2-(4-(Diphenylamino)Benzylidene) Malononitrile. *Crystals*, **15**, Article 380. https://doi.org/10.3390/cryst15040380

[58] Swain, C.K. and Scheiner, S. (2024) Comparison of Various Theoretical Measures of Aromaticity within Monosubstituted Benzene. *Molecules*, **29**, Article 2260. https://doi.org/10.3390/molecules29102260

[59] Nowakowska, Z. (2007) A Review of Anti-Infective and Anti-Inflammatory Chalcones. *European Journal of Medicinal Chemistry*, **42**, 125-137. https://doi.org/10.1016/j.ejmech.2006.09.019

[60] Zhuang, C., Zhang, W., Sheng, C., Zhang, W., Xing, C. and Miao, Z. (2017) Chalcone: A Privileged Structure in Medicinal Chemistry. *Chemical Reviews*, **117**, 7762-7810.

https://doi.org/10.1021/acs.chemrev.7b00020

[61] Morales-Reyna, M., Figueroa-Angulo, E.E., Espinoza-Hicks, J., Camacho-Dávila, A., López-Camarillo, C., Vázquez-Carrillo, L.I., *et al.* (2025) Prenylated Chalcones as Anticancer Agents against Castration-Resistant Prostate Cancer. *Scientia Pharmaceutica*, **93**, Article 25. https://doi.org/10.3390/scipharm93020025

[62] Sahu, K., Balbhadra, N.S., Choudhary, J. and Kohli, D.V. (2012) Exploring Pharmacological Significance of Chalcone Scaffold: A Review. *Current Medicinal Chemistry*, **19**, 209-225. https://doi.org/10.2174/092986712803414132

[63] Li, S. and Jin, H. (2025) Synthesis, Antibacterial Evaluation and Molecular Modeling of Novel Chalcone Derivatives Incorporating the Diphenyl Ether Moiety. *Molecules*, **30**, Article 2575. https://doi.org/10.3390/molecules30122575

[64] Conradie, J. (2025) The Use of DFT Methods to Predict the Reduction Potential of Chalcones. *Inorganica Chimica Acta*, **588**, Article 122866. https://doi.org/10.1016/j.ica.2025.122866